Combustion Science and Technology
Publication details, including instructions for authors and subscription information:
http://www.tandfonline.com/loi/gcst20

RADIATION EFFECTS FOR DOWNWARD FLAME SPREAD OVER A THERMALLY THIN FUEL IN A PARTIAL-GRAVITY ENVIRONMENT

KUO-KUANG WU [a] & CHIUN-HSUN CHEN [a]
[a] Department of Mechanical Engineering, National Chiao-Tung University , HsinChu, Taiwan, Republic of China
Published online: 11 Aug 2010.

To cite this article: KUO-KUANG WU & CHIUN-HSUN CHEN (2004) RADIATION EFFECTS FOR DOWNWARD FLAME SPREAD OVER A THERMALLY THIN FUEL IN A PARTIAL-GRAVITY ENVIRONMENT, Combustion Science and Technology, 176:11, 1909-1933, DOI: 10.1080/00102200490504553

To link to this article: http://dx.doi.org/10.1080/00102200490504553

Combust. Sci. and Tech., 176: 1909–1933, 2004

ISSN: 0010-2203 print/1563-521X online
DOI: 10.1080/00102200490504553

Taylor & Francis
Taylor & Francis Group

RADIATION EFFECTS FOR DOWNWARD FLAME SPREAD OVER A THERMALLY THIN FUEL IN A PARTIAL-GRAVITY ENVIRONMENT

KUO-KUANG WU AND CHIUN-HSUN CHEN*

Department of Mechanical Engineering, National Chiao-Tung University, HsinChu, Taiwan, Republic of China

This study explores the effects of radiation on a downward flame spread over a thermally thin solid fuel in a partial-gravity environment. The radiation effect and gravitational field strength (g) are predicted not to influence the ignition delay time. The flame-spread rate reaches a maximum at $g = 0.01$. At $g > 0.01$, the flame stretch effect dominates the behaviors of the flame. Radiation heat transfer and oxygen transport control the flame behaviors for $g < 0.01$. The predicted quenching limit is $g = 5 \times 10^{-6}$, close to the value obtained experimentally elsewhere. Radiation has two simultaneous effects. One is to reduce the flame strength by carrying heat to the ambient. The other one is combined with upstream conduction to enhance the total forward heat transfer rate and thus preheat virgin fuel upstream. The solid fuel temperature is low and some fuel is left over in low gravity due to radiation loss. Energy analyses indicate that the conduction heat flux from the flame ($\overline{q_c}$) dominates its behaviors. However, radiation gradually competes with $\overline{q_c}$ as the gravity is reduced.

Keywords: flame spread, partial gravity, radiation effect

Received 15 July 2003; accepted 29 March 2004.

The authors would like to thank the National Science Council of the Republic of China for financially supporting this research under Contract no. NSC89-2212-E009-058.

*Address correspondence to chchen@mail.nctu.edu.tw

INTRODUCTION

In an earlier study (Wu and Chen, 2003), the development of a flame from ignition to steady spread over a thermally thin solid fuel in a gravitational field was studied in detail. A parametric study predicted that the flame-spread rate increases as gravitational field strength declines in a partial-gravity environment ($g < 1$). However, this result contradicts the experimental findings of Olson et al. (1988) and Sacksteder and T'ien (1994), who found that the flame-spread rate is low in a partial-gravity environment. The study (Wu and Chen, 2003) neglected radiation, but this mode of heat transfer is crucial at low gravity. Therefore, this work addresses the effects of radiation on the downward flame spread over a thermally thin solid fuel in a partial-gravity environment.

Nakamura et al. (2000) numerically studied the ignition of a horizontal solid fuel heated by external radiation. They also considered solid radiation. They identified two distinct types of ignition. The first occurs when the oxygen concentration is relatively high and the flame is ignited at the tip of the plume with a short ignition delay. The second occurs when the oxygen concentration is low and ignition occurs inside the plume with a relatively long ignition delay. The first type of ignition is controlled by one-dimensional heat and mass transport, whereas the second type is controlled by a two-dimensional process caused by buoyancy-induced flow.

Chen and Cheng (1994) numerically studied the effect of radiative heat transfer on a downward flame spread over a thin fuel in low gravity. They used a two-flux model to approximate gas radiation in the cross-stream direction. They predicted that the effect of radiation becomes significant at $g < 0.05$ and extinction occurs when gravity is reduced to a critical value. However, at higher gravity, radiation is insignificant and the Damköhler number dominates. Lin and Chen (1999) considered two-dimensional gas radiation using a P-1 model as an approximation. They found the flame-spread trend, as observed in a previous study (Chen and Cheng, 1994). However, the flame spreads faster in higher gravity, because streamwise radiation preheats upstream virgin fuel, increasing the flame-spread rate.

Kumar et al. (2003) numerically studied the flame spread over a thin solid fuel in a forced-convection environment. They found that shortening the entrance accelerates the spread and reduces the oxygen-extinction limit in slow freestreams; however, the effects are reversed at

high freestream velocities. The length of the entrance affects the effective flow rate seen by the flame in the base region. This oppositely affects the radiation loss and the gas residence time, causing the crossover. Kumar et al. (2003) also compared the behaviors of opposed and concurrent flames. The flame-spread rate increases linearly with freestream velocity, but the opposed flame-spread rate increases to a peak and then decreases as the freestream velocity falls. At a given freestream velocity, the oxygen-extinction limits in concurrent flame are lower than in an opposed flame except in the very slow freestream regime. This crossover disappears if the freestream velocities are converted to relative velocities with respect to the flames.

In recent years, many numerical and experimental studies have been performed to explore the behaviors of flames in microgravity environments. In the low-velocity regime, the flame-spread rate of opposed flames increases with flow velocity to a maximum value before decreasing as the flow velocity is increased further (Fujita et al., 1997; Kashiwagi et al., 1996; Olson, 1991; Olson et al., 2001), because not enough oxygen cannot be transferred to the flame to support combustion as the flow velocity declines. If the flame initially propagates both upstream and downstream, the downstream flame will be extinguished by the ''oxygen shadow'' effect (McGrattan et al., 1996). As the flow velocity increases, the flame stretch effect becomes significant, reducing the flame-spread rate.

The main purpose of this study is to use an unsteady, two-dimensional combustion model coupled with a radiation model to clarify the effect of radiation on downward flame spread over a thermally thin cellulosic fuel in a partial-gravity environment. Analyses will determine the factor that dominates the behaviors of a flame in a partial-gravity environment.

MATHEMATICAL MODEL

Figure 1 presents the configuration of approach taken by this study, which is exactly the same as that used by Wu and Chen (2003). The assumptions made and normalization procedure applied are found in the literature (Wu and Chen, 2003) and are not repeated here. The mathematical model consists of continuity, momentum, energy, and species equations in the gas phase, and continuity and energy equations in the solid phase; the equations are coupled at the interface. Table 1 summarizes the governing equations. The model of radiation from gas is

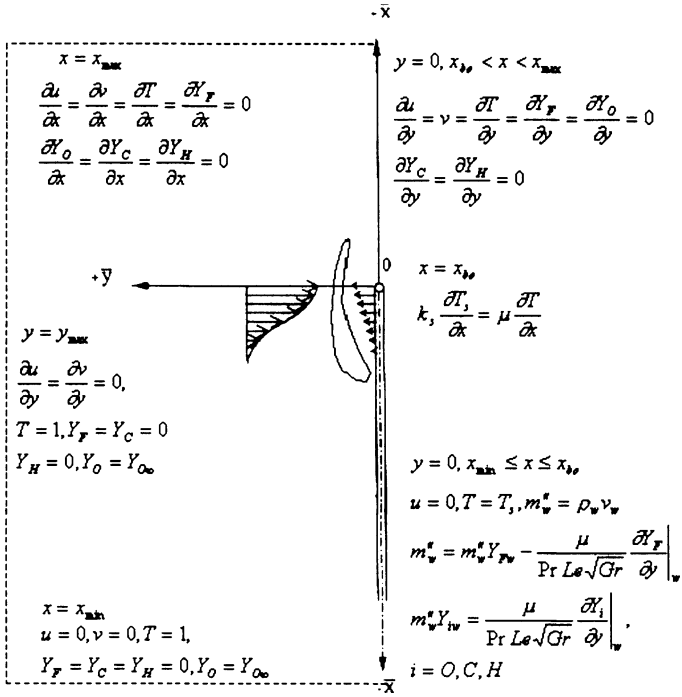

Figure 1. Schematic illustration of radiative ignition over a vertical solid fuel.

described in the following. The energy equations, which include the radiation term, differ from those in the cited previous study and are expressed as follows. For the gas phase,

$$\rho\frac{\partial T}{\partial t}+\rho u\frac{\partial T}{\partial x}+\rho v\frac{\partial T}{\partial y}=\frac{1}{Pr\sqrt{Gr}}\left[\frac{\partial}{\partial x}\left[\mu\frac{\partial T}{\partial x}\right]+\frac{\partial}{\partial y}\left[\mu\frac{\partial T}{\partial y}\right]\right]-q\dot{\omega}_{\mathrm{F}}-\frac{a}{N_\infty}(T^4-I_0) \tag{1}$$

where $a/N_\infty(T^4-I_0)$ is the gas radiation term. In the solid phase,

$$\rho_{\mathrm{s}}\frac{\partial T_{\mathrm{s}}}{\partial t}=\alpha_{\mathrm{s}}\frac{\partial^2 T_{\mathrm{s}}}{\partial x^2}+m''_{\mathrm{s}}\left[L+(1-C)(T_{\mathrm{s}}-1)\right]+\frac{\mu}{\tau Pr\sqrt{Gr}}\frac{\partial T}{\partial y}\bigg|_w+q_{\mathrm{ex}}+\frac{1}{\tau N_\infty}\left[\varepsilon\left(1-T_{\mathrm{s}}^4\right)+\frac{1}{3a}\frac{\partial I_0}{\partial y}\bigg|_w\right] \tag{2}$$

Table 1. Non-dimensional governing equations

Gas-Phase Governing Equation

$$\frac{\partial}{\partial t}(\rho\phi)+\frac{\partial}{\partial x}\left(\rho u\phi-\Gamma\frac{\partial\phi}{\partial x}\right)+\frac{\partial}{\partial y}\left(\rho v\phi-\Gamma\frac{\partial\phi}{\partial y}\right)=S$$

Equation	ϕ	Γ	S
Continuity	1	—	0
x Momentum	u	$\frac{\mu}{\sqrt{Gr}}$	$-\frac{\partial P}{\partial x}+S_u+\frac{\rho_\infty-\rho}{\rho_\infty-\rho_f}$
y Momentum	v	$\frac{\mu}{\sqrt{Gr}}$	$-\frac{\partial P}{\partial y}+S_v$
Energy	T	$\frac{\mu}{Pr\sqrt{Gr}}$	$-q\dot{\omega}_F-\frac{a}{N_\infty}(T^4-I_0)$
Fuel	Y_F	$\frac{\mu}{PrLe\sqrt{Gr}}$	$\dot{\omega}_F$
Other species $i=O_2,CO_2,H_2O$	Y_i	$\frac{\mu}{PrLe\sqrt{Gr}}$	$f_i\dot{\omega}_F$

Solid-Phase Governing Equations

Mass

$$m_s''=-\frac{\partial\rho_s}{\partial t}=A_s\rho_s\exp\left(-\frac{E_s}{T_s}\right)$$

Energy

$$\rho_s\frac{\partial T_s}{\partial t}=\alpha_s\frac{\partial^2T_s}{\partial x^2}+m_s''[L+(1-C)(T_s-1)]+\frac{\mu}{\tau\,\mathrm{Pr}\sqrt{Gr}}\frac{\partial T}{\partial y}\bigg|_w+q_{ex}+\frac{1}{\tau N_\infty}\left[\varepsilon\left(1-T_s^4\right)+\frac{1}{3a}\frac{\partial I_0}{\partial y}\bigg|_w\right]$$

where

$$S_u=\frac{1}{3}\frac{\partial}{\partial x}\left(\frac{\mu}{\sqrt{Gr}}\frac{\partial u}{\partial x}\right)+\frac{\partial}{\partial y}\left(\frac{\mu}{\sqrt{Gr}}\frac{\partial v}{\partial x}\right)-\frac{2}{3}\frac{\partial}{\partial x}\left(\frac{\mu}{\sqrt{Gr}}\frac{\partial v}{\partial y}\right)$$

$$S_v=\frac{1}{3}\frac{\partial}{\partial y}\left(\frac{\mu}{\sqrt{Gr}}\frac{\partial v}{\partial y}\right)+\frac{\partial}{\partial x}\left(\frac{\mu}{\sqrt{Gr}}\frac{\partial u}{\partial y}\right)-\frac{2}{3}\frac{\partial}{\partial y}\left(\frac{\mu}{\sqrt{Gr}}\frac{\partial u}{\partial x}\right)$$

$$\dot{\omega}_F=-Da\rho^2Y_FY_O\exp(-E/T)$$

Radiation transport equation: $\frac{\partial^2I_0}{\partial x^2}+\frac{\partial^2I_0}{\partial y^2}=-3a^2\left(T^4-I_0\right)$

Equation of state: $\rho\cong\frac{\gamma}{T}$

The equation for viscosity variation with temperature: $\mu=\frac{T}{\gamma}$

The last term in Eq. (2) is the radiation heat flux and includes the loss from the solid by radiation and radiated flux from the gas phase to the solid phase. Figure 1 presents the boundary conditions, which are initially as follows. For the gas phase,

$$t = 0 \quad u = v = 0 \quad T = 1 \quad Y_F = Y_C = Y_H = 0 \quad Y_O = Y_{O\infty} \tag{3}$$

For the solid phase,

$$t = 0 \quad \rho_s = T_s = 1 \tag{4}$$

This study also considers radiation from gas and solid. Some assumptions are made for radiation mode 1, as follows:

1. gas-phase radiation is two-dimensional.
2. The gas medium is optically thin and the scattering effect is not considered.
3. The participating media are CO_2 and H_2O.
4. Radiation from soot is neglected, based on experimental observations in conditions of slow flow and low oxygen concentrations (Grayson et al., 1994).
5. The fuel surface is opaque and diffuse.
6. The surface reflectivity is zero.

The P-1 approximation is used to describe the radiative heat flux (Lauriant, 1982). The nondimensional radiation transport equation is

$$\frac{\partial^2 I_0}{\partial x^2} + \frac{\partial^2 I_0}{\partial y^2} = -3a^2\left(T^4 - I_0\right) \tag{5}$$

where I_0 denotes the zeroth moment of radiation intensity and a is the effective mean absorption coefficient, which is defined as follows (Patch, 1967):

$$\overline{a} = \frac{\int_0^\infty \overline{a_\lambda I_{b\lambda}} \exp(-\overline{a_\lambda} S)\, d\lambda}{\int_0^\infty \overline{I_{b\lambda}} \exp(-\overline{a_\lambda} S)\, d\lambda} \qquad a = \overline{\delta a} \tag{6}$$

where $\overline{I_{b\lambda}}$ is the spectral blackbody intensity;$\overline{a_\lambda}$ is the spectral absorption coefficient, which is a function of temperature and the composition of the mixture; and S is the distance along the path of the radiation (overbars denote dimensional quantities). Ludwig et al. (1973) measured and

tabulated $\overline{a_\lambda}$. Marshak's boundary conditions (Marshak, 1947) apply to the transport equation and are presented as follows:

$$\left(1 - \frac{2}{3a}\frac{\partial}{\partial x}\right) I_0 = 1 \qquad \text{at } x = x_{\min} \tag{7}$$

$$\frac{\partial I_0}{\partial x} = 0 \qquad \text{at } x = x_{\max} \tag{8}$$

$$\left(1 - \frac{2}{3a}\frac{\partial}{\partial y}\right) I_0 = \varepsilon T_s^4 \quad \text{at } y = 0 \quad x_{\min} \le x \le x_{\text{bo}} \tag{9}$$

$$\frac{\partial I_0}{\partial y} = 0 \qquad \text{at } y = 0 \quad x_{\text{bo}} \le x \le x_{\max} \tag{10}$$

$$\left(1 - \frac{2}{3a}\frac{\partial}{\partial y}\right) I_0 = 1 \qquad \text{at } y = y_{\max} \tag{11}$$

Please refer to Ratzel and Howell (1983) for details of the radiation model.

The numerical scheme adopts the SIMPLE algorithm (Patankar, 1980). This model is solved using a marching time step. At each time step, the gas- and solid-phase equations are solved separately. Iteration is continued until all variables converge according to specified criteria, after which they are marched to the next time step. The subroutine RADCAL, developed by Grosshandler (1993), was modified and coupled with the present combustion model to obtain the effective absorption coefficient. The subroutine for radiation is executed once after 10 iterations during each time step. Grid points are clustered in the region heated by external radiation. A grid-size independence test was conducted in advance, and a time step of 0.02 s and a nonuniform 184×40 grid distribution were found to achieve an optimal balance among resolution, computational time, and memory requirements. The computation was performed on a PC at National Chiao-Tung University.

RESULTS AND DISCUSSION

The corresponding thermophysical properties and nondimensional parameter values are the same as in Wu and Chen's study (2003). Wu and

Chen (2003) detailed the entire flame development process, which is not repeated here.

Gravity slightly influences the ignition delay time, which is around 0.56 s. Notably, the ignition source in this study was a laser. The induced flow velocity is low in the heat-up stage so the flammable mixture can accumulate above the pyrolysis region and is not carried downstream. Therefore, the ignition delay time is controlled mainly by the time taken to form the flammable mixture and not by the induced flow strength, which is associated with gravity. As in a previous study (Wu and Chen, 2003) that ignored the effects of radiation, radiation did not influence the ignition delay time herein ($\overline{t_{ig}} \cong 0.56$ s). The low temperature in the heat-up stage is such that no radiation effect is evident. Table 2 lists the flame-spread rate ($\overline{V_f}$), the induced flow velocity ($\overline{V_r}$), the Damköhler number (Da), and the variation of the radiation to conduction parameter ($1/N_\infty$) with gravity. This table indicates that the flame-spread rate reaches a maximum ($\overline{V_f} = 0.839$ cm/s) at $g = 0.01$. The controlling mechanism at $g > 0.01$ differs greatly from that at $g < 0.01$. At $g > 0.01$, the flame stretch effect dominates the behaviors of the flame. The induced flow velocity increases (Da decreases) with gravity, so the forward heat transfer makes preheating the solid fuel increasingly difficult, reducing the flame-spread rate. In this regime, the effect of radiation is slight ($1/N_\infty = 0.021$ for $g = 1$) and radiation does not significantly influence the flame-spread rate. For $g < 0.01$, heat transfer by radiation and oxygen transport dominate the flame behaviors. The heat loss to the ambient by radiation increases significantly as gravity decreases (e.g., $1/N_\infty = 0.211$ for $g = 0.001$ and $1/N_\infty = 0.981$ for $g = 1 \times 10^{-5}$); hence, the flame becomes weaker. Clearly, if the radiation effect is not

Table 2. Effect of changing gravity level

g	$\overline{V_r}$ (cm/s)	$\overline{V_f}$ (cm/s)	$\frac{1}{N_\infty}$	Da
1.0	25.318	0.581	0.021	1.23×10^6
0.1	11.752	0.791	0.045	5.73×10^6
0.01	5.454	0.839	0.098	2.66×10^7
0.001	2.532	0.727	0.211	1.23×10^8
0.0005	2.009	0.623	0.266	1.96×10^8
0.0001	1.175	Unsteady	0.456	5.73×10^8
1.0×10^{-5}	0.545	Unsteady	0.981	2.66×10^9
5.0×10^{-6}	0.433	Extinction	1.236	4.22×10^9

considered, the flame becomes strong and the rate of spread increases continuously because the flame stretch effect weakens as gravity decreases. Moreover, the induced flow carries the oxygen into the flame. The induced flow velocity decreases as the gravity decreases (for example $\overline{V_r} = 25.32\,\mathrm{cm/s}$ for $g = 1$ and $\overline{V_r} = 1.175\,\mathrm{cm/s}$ for $g = 0.0001$). As the velocity of the induced flow decreases, the oxygen becomes harder to carry into the flame, causing the flame not to receive sufficient oxygen to support combustion. Ultimately, the flame is extinguished at $g = 5 \times 10^{-6}$ due to radiation loss and weak oxygen transport. These two factors will be discussed in detail later.

Sacksteder and T'ien (1994) performed experiments in a partial-gravity environment ($0.05 \leq g \leq 0.6$) and combined experimental data obtained in forced-convection environments (Ferkul, 1989; Olson, 1991; Olson et al., 1988) by changing the opposing flow velocities to the corresponding induced flow velocity $\overline{V_r} = [\overline{g}(\overline{\rho_\infty} - \overline{\rho_f})\overline{\alpha^*}/\overline{\rho^*}]^{1/3}$. They deduced that the flame would be extinguished in the range $10^{-6} \leq g \leq 10^{-5}$ for $Y_{O\infty} = 0.233$. The predicted quenching limit, $g = 5 \times 10^{-6}$, falls within this regime. The quenching limits predicted by Chen and Cheng (1994) and Lin and Chen (1999) are $g = 0.012$ and $g = 0.022$, respectively. These values are far from the experimental results because Chen and Cheng (1994) considered only cross-stream radiation, and Lin and Chen (1999) adopted the Plank mean absorption coefficient. Radiation not only carries heat away to the ambient but also preheats the solid fuel. Streamwise radiation preheats the solid fuel. The use of the Plank mean absorption coefficient may overpredict radiation emission (Bedir et al., 1997). Both streamwise and cross-stream radiations are considered herein to correct these drawbacks, and the effective absorption coefficient is adopted. Accordingly the prediction obtained herein is better than those obtained in previous studies.

Figures 2–4 illustrate the time sequence of isotherms and velocity vector distributions for $g = 1$, 0.01, and 0.0001, respectively. At $\bar{t} = 1$ s, the isotherm and velocity vector distributions at $g = 0.01$ and 0.0001 are very similar (Figures 2*b* and 2*c*). The flames are almost semicircular and the fluid flows outward. However, the isotherm and velocity vector distributions at $g = 1$ differ dramatically from those at $g = 0.01$ and 0.0001 (Figures 2*a*) because the time required to establish complete induced flow is short at $g = 1$; by this time, the induced flow is not established at $g = 0.01$ or 0.0001. As time passes, the discrepancies between temperature distribution and flow field gradually become apparent at various

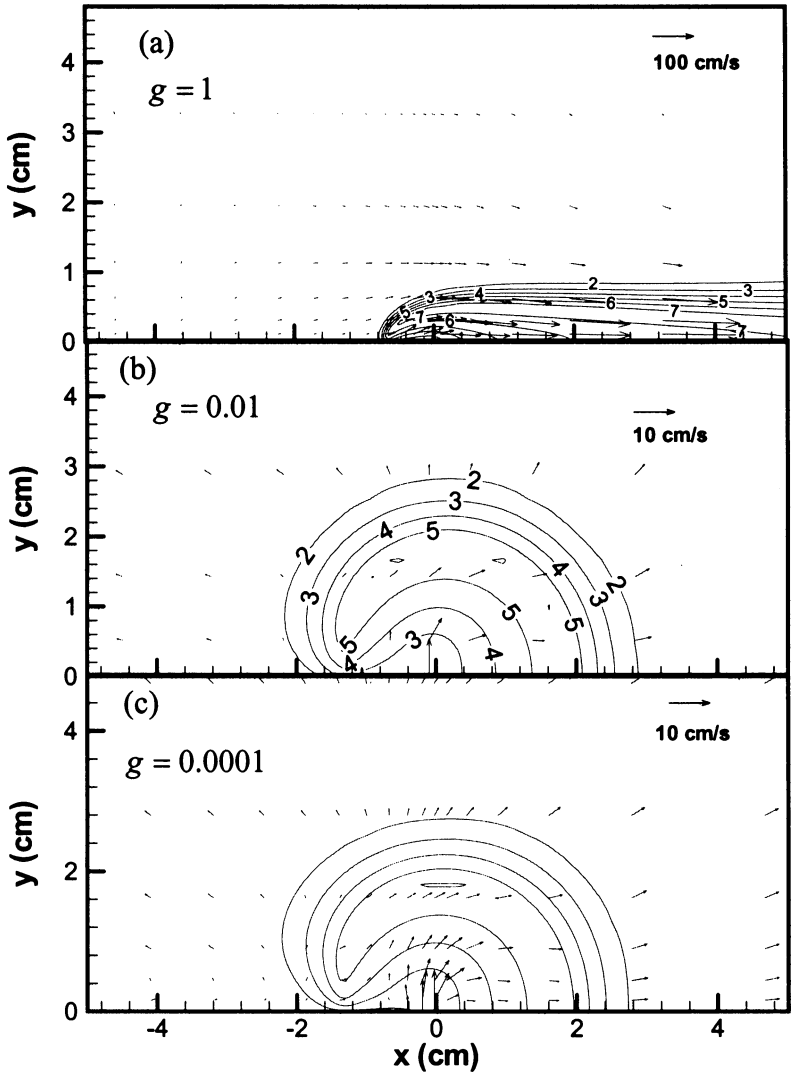

Figure 2. Isotherm and velocity vector distributions for $g = 1$, 0.01, and 0.0001 at $\bar{t} = 1$ s.

gravitational strengths. At $\bar{t} = 3$ s, the heated area (the area covered contour $T = 2$) increases as the gravity becomes weaker (Figures 3*a*–3*c*) but the gas-phase temperature decreases as gravity becomes weaker. Two factors—the velocity of induced flow and the effect of radiation—cause these phenomena. The induced flow velocity is proportional to $g^{1/3}$, so

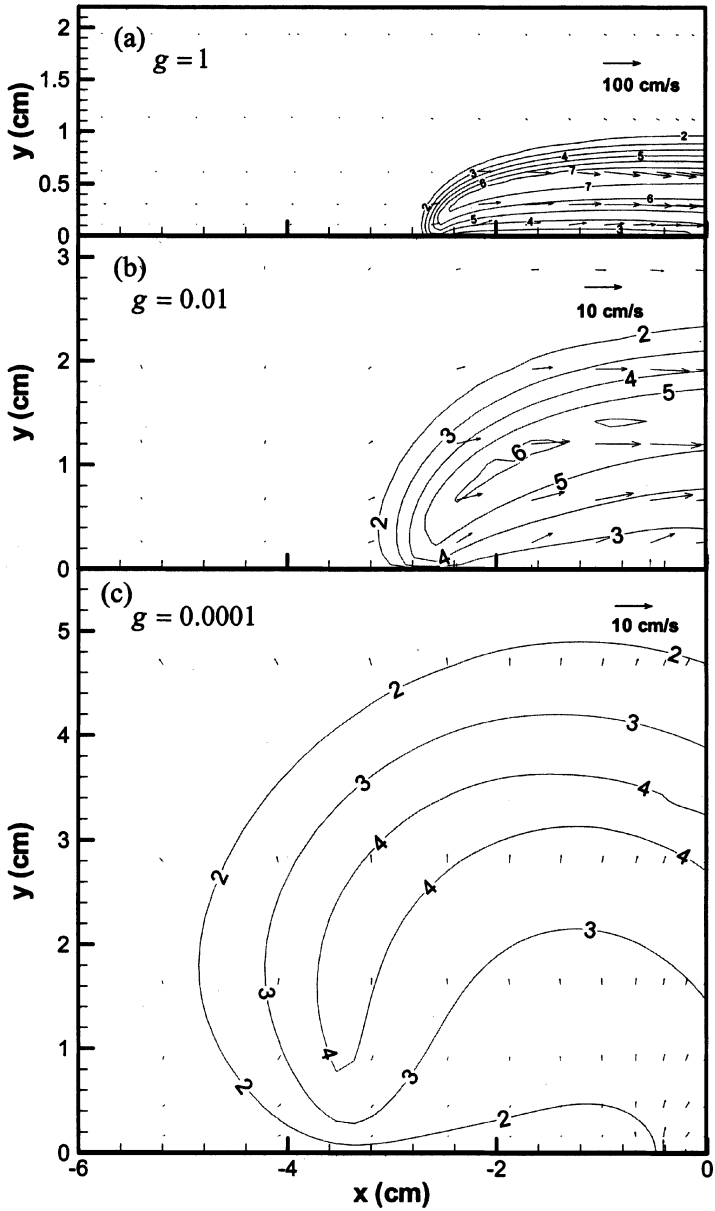

Figure 3. Isotherm and velocity vector distributions for $g = 1$, 0.01, and 0.0001 at $\bar{t} = 3$ s.

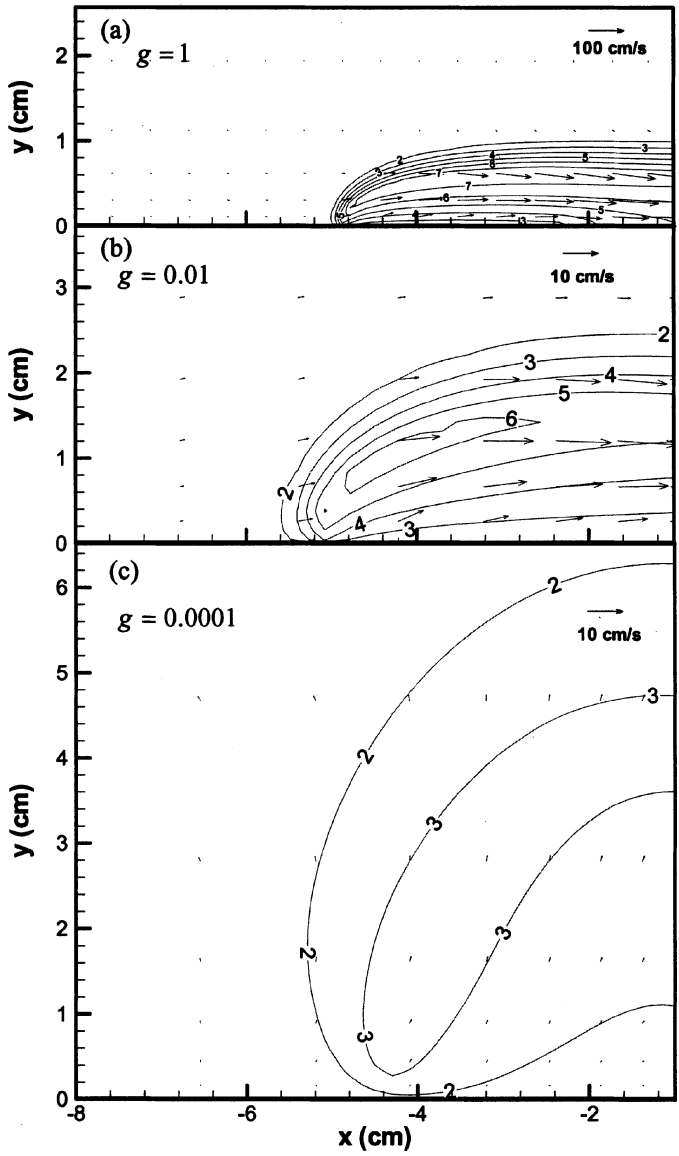

Figure 4. Isotherm and velocity vector distributions for $g = 1$, 0.01, and 0.0001 at $t = 6$ s.

the convective cooling effect becomes weaker as gravity decreases. Therefore, heat can be transferred farther via conduction. However, the magnitude of heat loss to the ambient by radiation increases as gravity

decreases. Hence, the gas-phase temperature is lower at lower gravity ($T_{max} = 7.65$ for $g = 1$ and $T_{max} = 4.54$ for $g = 0.0001$ at $\bar{t} = 3$ s). Ultimately, the flame reaches steady state at g = 1 and 0.01 (Figures 4*a* and 4*b*) but it cannot reach a steady state at $g = 0.0001$ until $\bar{t} = 6$ s (Figure 4*c*).

Figure 5 plots the fuel and oxygen mass fraction contour distributions at $g = 1$, 0.01, and 0.0001 at $\bar{t} = 6$ s. This figure reveals that the flame is a diffusion flame, except near the flame front where it is a premixed flame. The premixed flame region is a source for the ignition of the flammable mixture and thus supports the spread of the flame. Notably, the premixed flame region is not obvious at $g = 0.0001$ (Figure 5*c*). The transport of oxygen into the flame zone depends primarily on the induced flow strength. When the induced flow is weak, and when gravity is weak, the oxygen is more difficult to carry into the flame zone. If the oxygen supplied is insufficient to support combustion, then the flame becomes weaker and is eventually extinguished. This mechanism, called oxygen transport control, is another important cause of flame extinction in addition to loss due to radiation in low gravity.

Figure 6 plots contour at which the chemical reaction rate equals 10^{-4} g/cm^{3}s at $g = 1$, 0.01, and 0.0001 at $\bar{t} = 6$ s. These contours can be presented as a visible flame (Nakabe et al., 1994). The figure shows that the flame is shortest at $g = 0.0001$. Because of the slow induced flow, the flammable mixture is not carried downstream. The flame is largest at $g = 0.01$ where the flame-spread rate is maximum. The flame is small when $g = 0.0001$ for the following reason. The rate of chemical reaction is a function of temperature and oxygen and fuel concentrations ($\bar{\omega}_F = -\overline{B\rho}^2 Y_F Y_O \exp(-\overline{E}/\overline{RT})$). The transport of oxygen into the flame zone is difficult because the induced flow is weak in low gravity. Moreover, the amount of heat lost to the ambient by radiation becomes great and reduces the temperature of the flame. In the meantime, the standoff distance—the shortest distance between the flame and the surface of the solid fuel—increases, reducing the amount of energy transported from the flame to the solid fuel via gas-phase conduction, decreasing the rate of pyrolyzation of fuel vapor. Therefore, the flame is small in low gravity and becomes extinct as the gravity level is reduced further.

Figure 7 combines the isotherms combined and radiative heat flux vectors at $g = 1$, 0.01, and 0.0001 at $\bar{t} = 6$ s. The radiation has two forms. One reduces the strength of the flame, reducing its temperature, by loss of heat to the ambient (so the vectors point outward). This radiation reduced the energy fed back from the flame to the solid fuel, reducing the

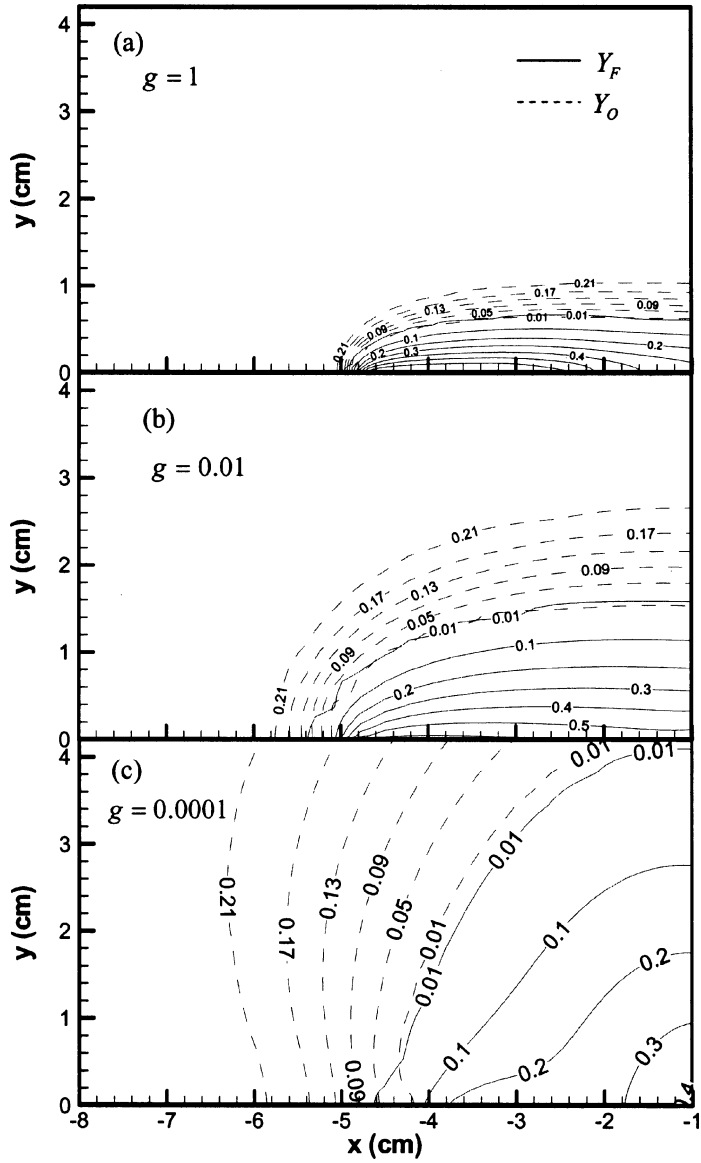

Figure 5. The fuel and oxygen mass fraction contour distributions for $g = 1$, 0.01, and 0.0001 at $\bar{t} = 6$ s.

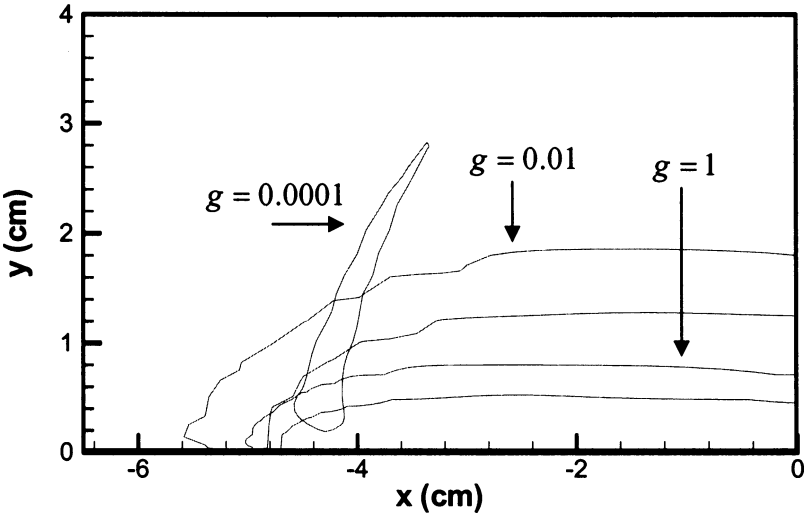

Figure 6. Constant contour distributions of chemical reaction rate equal to 10^{-4} g/cm^{3}s for $g = 1$, 0.01, and 0.0001 at $\bar{t} = 6$ s.

flame-spread rate. The other form is radiation that joins upstream conduction to reinforce the total forward heat transfer and the subsequent preheating of the upstream virgin fuel (so these vectors point toward the surface of the fuel). This effect causes the solid fuel to more easily pyrolyze the fuel vapor, accelerating the flame spread. These two contributions compete with each other. Figures 7*a*–7*c* indicate that radiation effects are greater at lower gravity despite the loss of heat to the ambient or the preheating of solid fuel. This finding confirms that radiation does not dominate behaviors of a downward flame in an elevated-gravity environment. Clearly, the effect of radiation loss from the flame to the ambient exceeds that of the preheating of the solid fuel in low gravity, reducing the flame-spread rate (Table 2).

Figure 8 plots the nondimensional solid temperature (T_s) profiles for $g = 1$, 0.01 and 0.0001 at $\bar{t} = 6$ s. In the preheated zone, forward heat conduction and radiation from the flame preheats the solid fuel. All of the received energy is used to raise the temperature of the solid fuel in this zone. The rate of increase of the temperature is high near the leading edge of the flame because the part of the flame closest to the solid fuel feeds back much energy to the solid fuel. After T_s reaches its peak value, it decreases because most of the received energy is used to pyrolyze the solid

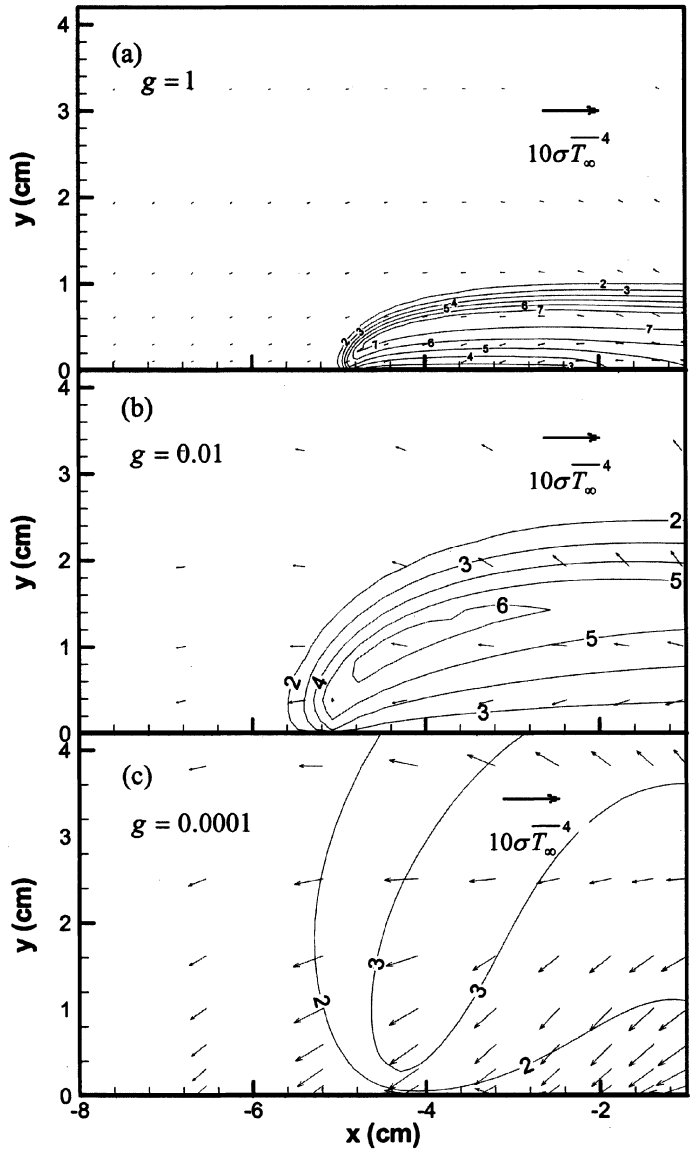

Figure 7. Isotherm and radiative flux vector distributions for $g = 1$, 0.01, and 0.0001 at $\bar{t} = 6$ s.

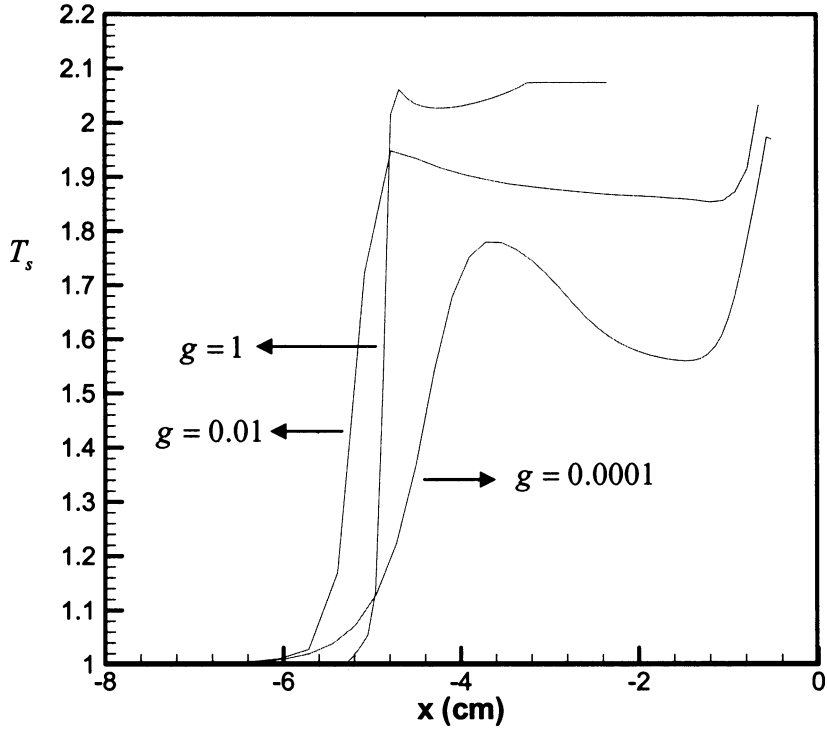

Figure 8. The nondimensional solid temperature profiles for $g = 1$, 0.01, and 0.0001 at $\bar{t} = 6$ s.

fuel into vapor such that no more energy can be used to raise the temperature. Notably, T_s increases again near the origin except at $g = 1$, because the external radiant source heats the solid fuel continuously. At $g = 1$, the solid fuel is burned out, and so it is not affected by the external radiant source. As shown in Figure 8, T_s decreases as gravity decreases because of the amount of energy fed back from the flame to the solid fuel. Weaker gravity corresponds to the feeding back of less energy to the solid fuel. The heat flux will be discussed in detail later.

Figure 9 plots the nondimensional solid density (ρ_s) profiles at $g = 1$, 0.01, and 0.0001 at $\bar{t} = 6$ s. The density profiles have two valleys—one near the origin and the other one near the flame front—because heat absorbed by the solid fuel comes from two sources: the external radiant flux and the flame itself. The external radiant flux has a Gaussian distribution, whose half-width is 0.5 cm and whose peak is 5 W/cm^2; it heats

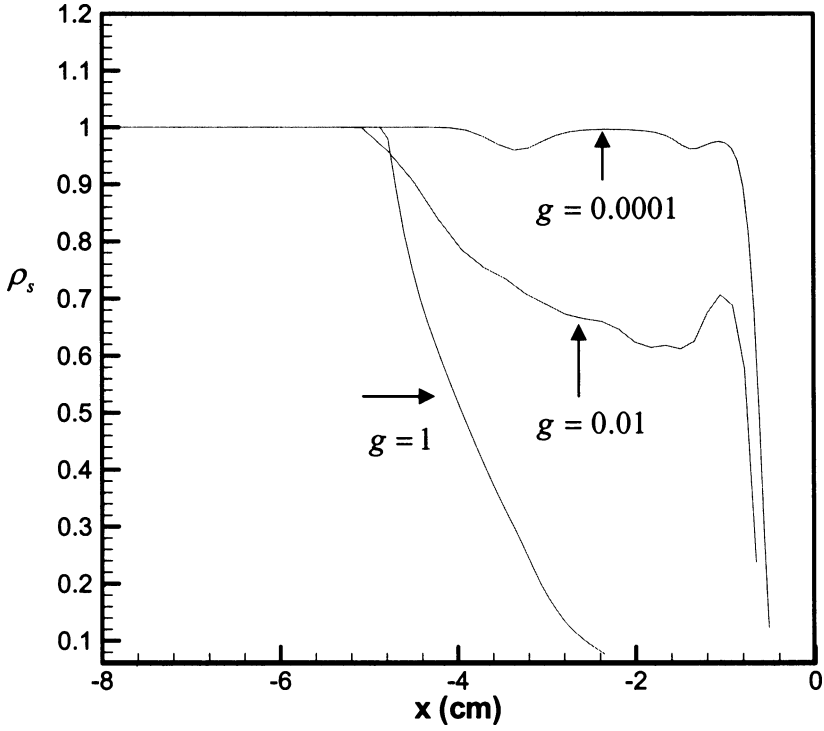

Figure 9. The non-dimensional solid density profiles for $g = 1$, 0.01, and 0.0001 at $\bar{t} = 6$ s.

the solid fuel continuously until burnout. Therefore, the valley near the origin is very deep. Nakamura et al. (2002) predicted the same phenomenon in a forced-convection environment. As shown in Figure 9, ρ_s varies less when gravity is weaker, implying that the solid fuel does not pyrolyze completely and so some solid fuel is left over downstream of the flame. The amount of leftover fuel increases as the gravity becomes weaker, and so the variation in density is less. However, no fuel is left in stronger gravity ($g = 1$). The amount of energy fed back from the flame to the solid fuel decreases as gravity increases. Radiation losses are more apparent at lower gravity. Hence, the solid fuel cannot receive sufficient heat to pyrolyze fuel vapor continuously and so the solid fuel is retained. Bhattacharjee et al. (1993) and Ramachandra et al. (1995) experimentally observed this phenomenon in a microgravity environment, and Kumar et al. (2003) numerically predicted this phenomenon in a weakly forced flow environment.

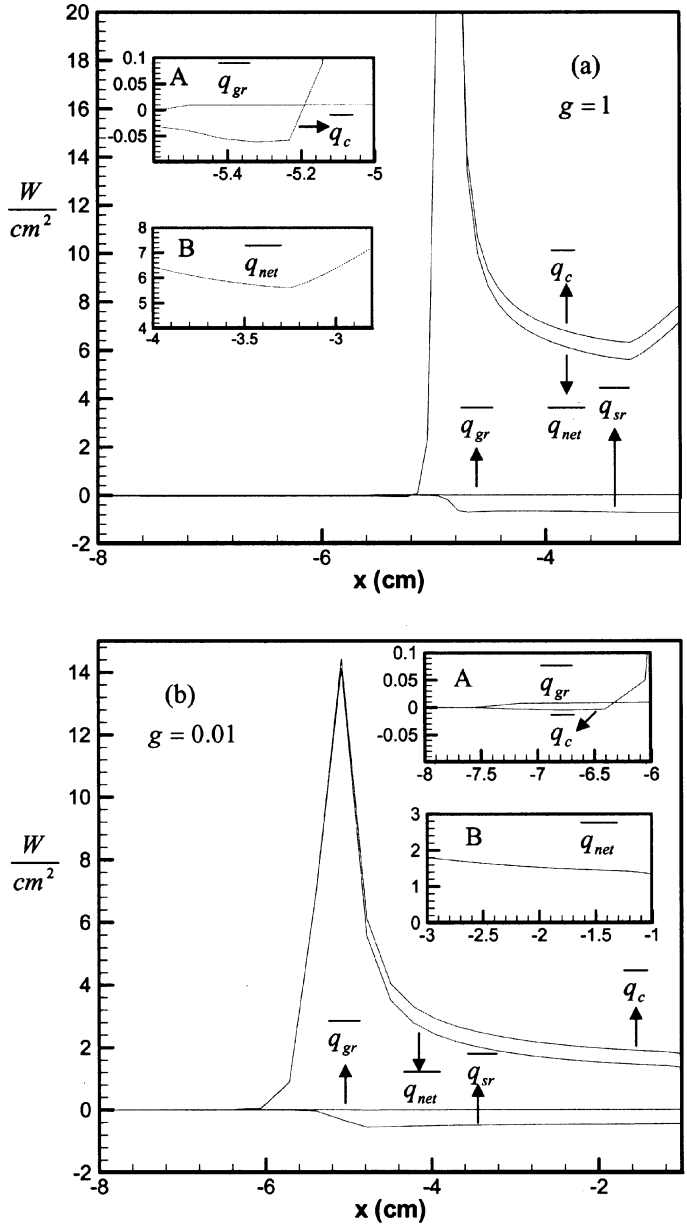

Figure 10. The heat flux distributions include the conduction heat flux from the gas ($\overline{q_c}$), gas-phase radiation feedback ($\overline{q_{gr}}$), radiation heat loss from the solid fuel ($\overline{q_{sr}}$), and net heat flux ($\overline{q_{net}}$) for $g = 1$, 0.01, and 0.0001 at $\bar{t} = 6$ s.

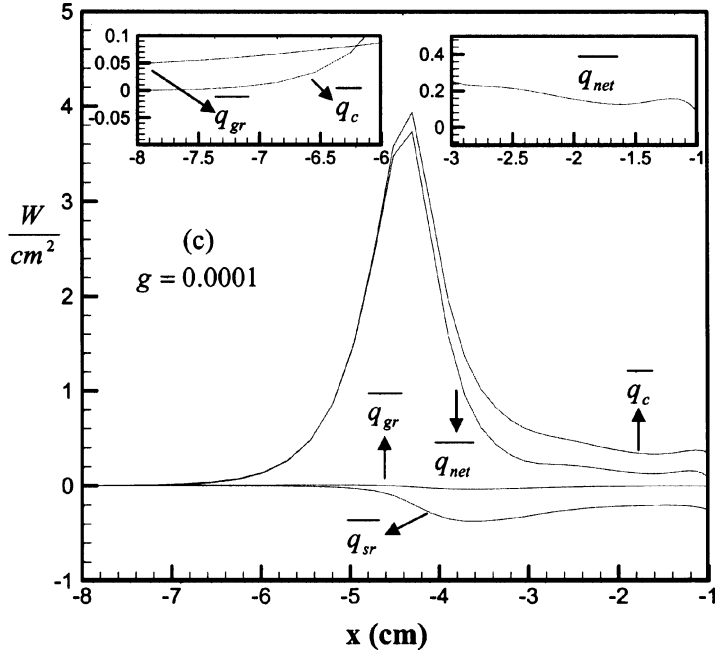

Figure 10. Continued.

Figure 10 presents the heat flux distributions, including the conduction heat flux from the gas ($\overline{q_c}$), the gas-phase radiation feedback ($\overline{q_{gr}}$), the radiation heat loss from the solid fuel ($\overline{q_{sr}}$), and the net heat flux ($\overline{q_{net}}$) at $g = 1$, 0.01, and 0.0001 at $\bar{t} = 6$ s. A positive value indicates that the solid fuel gains energy from the gas phase and a negative value represents heat lost from the surface of the solid fuel. This figure reveals that $\overline{q_c}$ is the major contribution to the energy feedback; $\overline{q_c}$ is concentrated around the leading edge of the flame, which is the part of the flame closest to the solid fuel. As shown in insets A of Figure 10*a*–10*c*, $\overline{q_{gr}}$ preheats the solid fuel farther upstream while $\overline{q_c}$ represents heat loss; $\overline{q_{sr}}$ is the major heat loss term. Since $\overline{q_{sr}}$ is proportional to T_s^4, it is large behind the flame's leading edge. West et al. (1992) also indicated that radiation from the solid considerably influences the flame-spread rate in low gravity. The magnitude of $\overline{q_{net}}$—the sum of $\overline{q_c}$, $\overline{q_{gr}}$, and $\overline{q_{sr}}$—reaches a maximum around the leading edge of the flame because $\overline{q_c}$ is large there. Although the loss of heat to the ambient by radiation in weak gravity weakens the flame, it increases the energy feedback via radiation (see inset A of Figure 10*a*–10*c*). However, energy feedback via

conduction is reduced. These two effects compete with each other. Apparently, the latter effect dominates the former one, and so $\overline{q_{\text{net}}}$ decreases sharply as gravity decreases in spite of the greater $\overline{q_{\text{gr}}}$ and consequently enhanced preheating of solid fuel in weak gravity. Behind the leading edge of the flame, $\overline{q_{\text{net}}}$ approaches zero (inset B of Figure 10*a*–10*c*) so sufficient energy cannot be supplied to pyrolyze solid fuel and raise its temperature. Therefore, fuel is left over and T_{s} is low at low gravity (Figures 8 and 9).

CONCLUSIONS

This work numerically studies the effects of radiation on downward flame spread over a thermally thin solid fuel in a partial-gravity environment. Both streamwise and cross-stream radiations are considered and the effective absorption coefficient is adopted. The effects of radiation and gravity are predicted to weakly influence the ignition delay because induced flow is not established and the temperature is low in the heat-up stage. The rate of flame-spread rate reaches a maximum at $g = 0.01$. At $g > 0.01$, the flame stretch effect dominates the behaviors of the flame. The induced flow velocity increases with gravity so the forward heat transfer becomes less able to preheat the solid fuel, reducing the flame-spread rate. At $g < 0.01$, the radiation heat transfer and oxygen transport dominate the flame behaviors. The loss of heat to the ambient by radiation increases significantly as gravity decreases. Moreover, slower induced flow corresponds to greater difficulty with which oxygen is carried into the flame. Based on these two factors, the flame becomes weak and the spread rate is reduced. The predicted quenching limit is $g = 5 \times 10^{-6}$—close to the experimental value (Sacksteder and T'ien, 1994).

Two distinct radiative effects apply. The first reduces the flame strength by carrying heat to the ambient. The other joins the upstream conduction and reinforces the total forward heat transfer rate and the subsequent preheating of upstream virgin fuel. These two contributions compete with each other. The former overcomes the latter at low gravity, resulting in a low solid temperature and causing fuel to be left over. Energetic analyses indicate that the conduction heat flux from the flame dominates the flame behaviors. However, the radiation effect gradually competes with the conduction heat flux from the flame as the gravity decreased further.

The radiation model is coupled with the present combustion model, and so the execution time is very long. Parallel computation will be used to overcome this difficulty and thus support advanced research in the future.

NOMENCLATURE

A_s nondimensional preexponential factor for fuel pyrolysis, $\overline{A_s}\,\overline{\alpha^*}\Big/\overline{V_r}^2$
$\overline{B}$ preexponential factor for gas-phase reaction, $\mathrm{cm}^3/\mathrm{mol}\cdot\mathrm{s}$
C specific heat ratio of the gas mixture to solid fuel, $\overline{C_p}/\overline{C_s}$
$\overline{C_p}$ specific heat for gas mixture, J/gK
$\overline{C_s}$ specific heat for solid fuel, J/gK
$\overline{D}$ specific diffusivity, cm^2/s
Da Damköhler number, $\bar{B}\overline{\rho^*}\bar{\delta}/\overline{V_r}$
E nondimensional activation energy, $\overline{E}/\overline{R}\;\overline{T_\infty}$
f stoichiometric oxidizer/fuel mass ratio
g nondimensional gravitational acceleration, $\overline{g}/\overline{g_e}$
$\overline{g_e}$ Earth normal gravity, cm/s^2
Gr Grashof number, $\overline{g}(\overline{\rho_\infty}-\overline{\rho_f})\bar{\delta}^3\Big/\overline{\rho^* v^*}^2$
k_s nondimensional solid-phase conductivity, $\overline{k_s}/\overline{k}^*$
L nondimensional latent heat, $\bar{L}/\overline{C_s T_\infty}$
Le Lewis number, $\bar{\alpha}/\bar{D}$
m_s'' nondimensional mass flux, $\overline{m_s''\alpha^*}/\overline{\rho_{s\infty}V_r}^2\bar{\tau}$
N_∞ conduction-radiation parameter based on $\overline{T_\infty}$, $\overline{k^*V_r}/\overline{\sigma T_\infty}^3\overline{\alpha^*}$
P nondimensional pressure, $(\overline{P}-\overline{P_\infty})/\overline{\rho^* V_r}^2$
Pr Prandtl number, $\bar{\nu}/\bar{\alpha}$
q nondimensional heat of combustion per unit mass of fuel, $\overline{q}/\overline{C_p T_\infty}$
q_{ex} nondimensional external heat flux, $\overline{q_{ex}}\,\overline{\alpha^*}/\overline{\tau\rho_{s\infty}C_s T_\infty V_r}^2$
$\overline{R}$ universal gas constant, J/mol·K
t nondimensional time, $\bar{t}\overline{V_r}^2/\overline{\alpha^*}$
T nondimensional gas-phase temperature, $\bar{T}/\overline{T_\infty}$
T_s nondimensional solid-phase temperature, $\overline{T_s}/\overline{T_\infty}$
u nondimensional velocity parallel to the fuel surface, $\bar{u}/\overline{V_r}$
v nondimensional velocity normal to the fuel surface, $v/\overline{V_r}$
$\overline{V_r}$ reference velocity, $[\bar{g}(\overline{\rho_\infty}-\overline{\rho_f})\overline{\alpha^*}/\overline{\rho^*}]^{1/3}$
$\overline{V_f}$ flame-spread rate, cm/s
x nondimensional distance parallel to the fuel surface, $\bar{x}/\bar{\delta}$
x_{bo} burnout position
y nondimensional distance normal to the fuel surface, $\bar{y}/\bar{\delta}$
Y_F fuel mass fraction
Y_O oxygen mass fraction
$\overline{\alpha}$ thermal diffusivity, cm^2/s

γ temperature ratio, $\overline{T^*}/\overline{T_\infty}$
$\overline{\delta}$ reference length $\overline{\alpha^*}/\overline{V_r}$, cm
ε emissivity
μ nondimensional dynamic viscosity, $\overline{\mu}/\overline{\mu^*}$
$\overline{v}$ kinematic viscosity, cm^2/s
ρ nondimensional density of gas phase, $\overline{\rho}/\overline{\rho^*}$
ρ_s nondimensional density of solid phase, $\overline{\rho_s}/\overline{\rho_{s\infty}}$
τ nondimensional solid fuel half-thickness, $\bar{\tau}\overline{C_s\rho_{s\infty}V_r}/\overline{k^*}$
$\dot{\omega}_F$ nondimensional gas-phase reaction rate, $-Da\rho^2 Y_F Y_O \exp(-E/T)$

Superscripts

$''$ flux
$*$ reference state

Subscripts

C carbon dioxide
ex external
F gaseous fuel
H water vapor
max location of downstream boundary
min location of upstream boundary
O oxidizer
s solid phase
∞ ambient condition

REFERENCES

Bedir, H., T'ien, J.S., and Lee, H.S. (1997) Comparison of different radiation treatments for a one-dimensional diffusion flame. *Combust. Theory Model.*, **1**, 395–404.

Bhattacharjee, S., Altenkirch, R.A., and Sacksteder, K. (1993) Implications of spread rate and temperature measurements in flame spread over a thin fuel in a quiescent, microgravity, space-based environment. *Combust. Sci. Technol.*, **91**, 225–242.

Chen, C.H. and Cheng, M.C. (1994) Gas-phase radiative effects on downward flame spread in low gravity. *Combust. Sci. Technol.*, **97**, 63–83.

Ferkul, P.V. (1989) *An Experimental Study of Opposed Flow Diffusion Flame Extinction over a Thin Fuel in Microgravity*. NASA CR-182185.

Fujita, O., Kikuchi, M., Ito, K., Olson, S.L., Kashiwagi, T., and Sakuraya, T. (1997) Observation of ignition and flame spread of paper sheet in slow external flow under microgravity. *J. Jpn Appl. Micrograv. Soc.*, **14**, 25–33.

Grayson, G., Sacksteder, K.R., Ferkul, P.V. and T'ien, J.S. (1994) Flame spreading over a thin solid in low-speed concurrent flow-drop tower experimental results and comparison with theory. *Micrograv. Sci. Technol.*, **7**, 187–195.

Grosshandler, W.L. (1993) *RADCAL: A Narrow-Band Model for Radiation Calculations in a Combustion Environment*. NIST Technical Note 1402.

Kashiwagi, T., McGrattan, K.B., Olson, S.L., Fujita, O., Kikuchi, M., and Ito, K. (1996) Effects of Slow Wind on Localized Radiative Ignition and Transition to Flame Spread in Microgravity. *Proc. Combust. Instit.*, **26**, 1345–1352.

Kumar, A., Shih, H.Y., and T'ien, J.S. (2003) A comparison of extinction limits and spreading rates in opposed and concurrent spreading flames over thin solids. *Combust. Flame*, **132**, 667–677.

Lauriant, G. (1982) Combined radiation-convection in gray fluids enclosed in vertical cavities. *J. Heat Transf.*, **104**, 609–615.

Lin, T.H. and Chen, C.H. (1999) Influence of two-dimensional gas phase radiation on downward flame spread. *Combust. Sci. Technol.*, **141**, 83–106.

Ludwig, C., Malkmus, W., Reardon, J., and Thomson, J. (1973) *Handbook of Infrared Radiation from Combustion Gases*. NASA SP-3080.

Marshak, R.E. (1947) Note on the spherical harmonics method as applied to the milne problem for a sphere. *Phys. Rev.*, **71**, 443–446.

McGrattan, K.B., Kashiwagi, T., Baum, H.R., and Olson, S.L. (1996) Effects of ignition and wind on the transition to flame spread in a microgravity environment, *Combust. Flame*, **106**, 377–391.

Nakabe, K., McGrattan, K.B., Kashiwagi, T., Baum, H.R., Yamashita, H., and Kushida, G. (1994) Ignition and transition to flame spread over a thermally thin cellulosic sheet in a microgravity environment, *Combust. Flame*, **98**, 361–374.

Nakamura, Y., Yamashita, H., Takeno, T., and Kushida, G. (2000) Effects of gravity and ambient oxygen on a gas-phase ignition over a heated solid fuel. *Combust. Flame*, **120**, 34–48.

Nakamura, Y., Kashiwagi, T., Mcgrattan, K.B., and Baum, H.R. (2002) Enclosure effects on flame spread over solid fuels in microgravity. *Combust. Flame*, **130**, 307–321.

Olson, S.L. (1991) Mechanisms of microgravity flame spread over a thin solid fuel: Oxygen and opposed flow effects, *Combust. Sci. Technol.*, **76**, 233–249.

Olson, S.L., Ferkul, P.V., and T'ien, J.S. (1988) Near-Limit Flame Spread over a Thin Solid Fuel in Microgravity, *Proc. Combust. Instit.*, **22**, 1213–1222.

Olson, S.L., Kashiwagi, T., Fujita, O., Kikuchi, M., and Ito, K. (2001) Experimental observations of spot radiative ignition and subsequent three-

dimensional flame spread over thin cellulose fuels, *Combust. Flame*, **125**, 852–864.

Patankar, S.V. (1980) *Numerical Heat Transfer and Fluid Flow*, McGraw-Hill, New York.

Patch, R.W. (1967) Effective absorption coefficients for radiant energy transport in nongrey, nonscattering gases, *J. Quant. Spectrosc. Rad.*, **7**, 611–637.

Ramachandra, P.A., Altenkirch, R.A., Bhattacharjee, S., Tang, L., Sacksteder, K., and Wolverton, M.K. (1995) The behavior of flames spreading over thin solids in microgravity, *Combust. Flame*, **100**, 71–84.

Ratzel, C., III and Howell, J.R. (1983) Two-dimensional radiation in absorbing-emitting media using the P-N approximation, *J. Heat Transf.*, **105**, 333–340.

Sacksteder, K.R. and T'ien, J.S. (1994) Buoyant Downward Diffusion Flame Spread and Extinction in Partial-Gravity Accelerations, *Proc. Combust. Instit.*, **25**, 1685–1692.

West, J., Bhattacharjee, S., and Altenkirch, R.A. (1992) A comparison of the roles played by natural and forced convection in opposed-flow flame spreading, *Combust. Sci. Technol.*, **83**, 233–244.

Wu, K.K. and Chen, C.H. (2003) A numerical analysis of ignition to steady downward flame spread over a thin solid fuel, *Combust. Sci. Technol.*, **175**, 933–964.